RSC Advances

COMMUNICATION

View Article Online
View Journal | View Issue

Cite this: *RSC Adv.*, 2014, **4**, 46976

Clay nanomaterial thin film electrodes for electrochemical energy storage applications†

M. Fatnassi, C.-H. Solterbeck and M. Es-Souni*

Received 9th May 2014
Accepted 19th September 2014

DOI: 10.1039/c4ra04330h

www.rsc.org/advances

Thin films of the smectite clay nanomaterial Laponite and nanocomposites thereof are suitable for high performance supercapacitors. With a maximum specific capacitance of 130 F g^{-1}, high retention rate and long-term stability, Laponite based electrodes perform as well as their carbon-counterparts while affording the advantages of low-cost and environmental friendliness.

Clays are seminal to human civilization, and it is even speculated upon that they may have acted as vectors to the formation of complex molecules in soil thus allowing development of biological life.[1] But beyond their known use in pottery, clay materials play an important role in industrial processes, and more recently they have emerged as promising high-tech nanomaterials for drug delivery, catalyst and catalyst supports, soil and waste-water purification, and as additives to polymeric materials to tune their physical properties.[2–6] Laponite nanomaterial that constitutes the main subject of study in the present communication is synthetic smectite clay with the general formula $Na_{0.7}^{+}[(Si_8Mg_{5.5}Li_{0.3})O_{20}(OH)_4]^{-0.7}$; its structure, displayed in Fig. ESI-2 (ESI†), consists of parallel sheets of tetrahedrally coordinated silica and octahedrally coordinated magnesium oxide sandwiched between them.[7] A fraction of divalent magnesium is substituted by monovalent Li which results in a net negative charge on the surface; sodium ions in the interlayer structure compensate the negative charge and ensure electrostatic cohesion of the layered structure. Laponite is available as nanosized particles in nearly monodisperse quality (Laponite RD®). The cylindrical nanoparticles resemble flat coins with a diameter of approximately 25 nm and 1 nm thickness (see Fig. ESI-2†). Laponite is easily modified by intercalating molecules such as silanes to generate additional properties such as hydrophobicity and affinity for adsorbents; eventually the intercalated molecules can expand the layered structure to such a degree that exfoliation occurs (separation of the individual layers) subsequently yielding functionalized leaflets with high surface area.[8]

Clay materials have been considered in few publications as supports for carbon nanomaterials, including graphene, for energy storage applications, but have not been considered before as the active electrode materials for electrochemical double layer capacitors.[9] We will show in the course of this communication that Laponite and more generally smectite clays can yield highly cost-effective, low carbon foot-print supercapacitor electrodes. The specific capacitance of these Laponite film electrodes may even be further boosted by intercalating some organo-silanes, exemplary shown on trihydroxysilylpropyl-methylphosphonate, to yield Laponite–organosilane-nanocomposites.

Two sample series were fabricated *via* dip coating of Au-terminated silicon substrates. The first series consisted of pure Laponite films, the second of Laponite–trihydroxysilylpropyl-methylphosphonate nanocomposite.

High-resolution scanning electron microscopy images show for both sample series nanocrystalline films with typical particle sizes in the range from 30 to 80 nm for the Laponite film, Fig. 1a, and a rather finer structure for the nanocomposite film (Fig. ESI-3†). The cross section micrograph displayed in Fig. 1b reveals that the films are built-up of leaflet stacks with few nanometers thickness. The arrangement of the nanoparticles in the film is probably of the well-known T-type, or edge-to-face bonds as it arises from the electrostatic interaction between the positively charged particle rim and the negatively charged surface; the scanning transmission micrographs, Fig. 1c and d, indeed show that this is probably the case, with the formation of a far more finer network for the nanocomposite film.[10] More details of the film morphology can be obtained using AFM, Fig. 2. The amplitude image, Fig. 2a, displays rather smooth films with an overall root mean square (rms) roughness of 15 nm (Fig. ESI-4†). A close look at the phase image, Fig. 2b, reveals that the particles assemble face-up in the outer layer of

Institute for Materials & Surface Technology, University of Applied Sciences Kiel, Germany. E-mail: me@fh-kiel.de

† Electronic supplementary information (ESI) available. See DOI: 10.1039/c4ra04330h

the plain Laponite film while again finer structures are obtained for the nanocomposite film, Fig. 2c.

The XRD patterns of Laponite powder, Laponite and nanocomposite films are displayed in Fig. 3. The complete series of Bragg reflections observed on the powder diagram correspond to Laponite structure-like clay with random orientation of particles.[11]

The XRD patterns of the Laponite and nanocomposite films differ from those of the corresponding powder. In particular, significant differences are noticed for the 001 reflection that is better defined for the Laponite films. The full width at half-maximum (FWHM) of the 001 peak is 4.29° for the Laponite powder and decreases to 3.29° for the Laponite film. This means that the (001) plane of the particle sheets is perpendicular to the substrate. Moreover, the peak positions of the nanocomposite film shifts to lower Bragg angles. More particularly, the 001 peak (2Θ = 5.5–7°), corresponding to the lattice spacing along the (001) plane, d_{001}, of the silicate layer in Laponite is shifted from $2\Theta = 6.33°$ (Laponite powder) to $2\Theta = 5.78°$ (nanocomposite film).[12] Using the Bragg's equation, the corresponding increase in the d_{001} is 1.41 nm for the Laponite film to 1.53 nm in the nanocomposite sample, suggesting that some of the phosphonate organosilane is intercalated between the Laponite layers (see Fig. ESI-2†).

Additional information about the structure of the synthesized Laponite–phosphonate nanocomposite were obtained from Raman and FT-IR spectroscopy and are described in the ESI (Fig. ESI-5 and 6†).

Based on the XRD data and the Raman spectra we may state that a fraction of the organosilane is intercalated into the Laponite layer, probably following the mechanism reported by Herrera *et al.*[13] who suggest that for trifunctional silanes the intercalation of polysiloxane oligomers may start by grafting at the edge of Laponite and, depending on concentration, penetrates the interior of the particles thus increasing the interlamellar spacing.

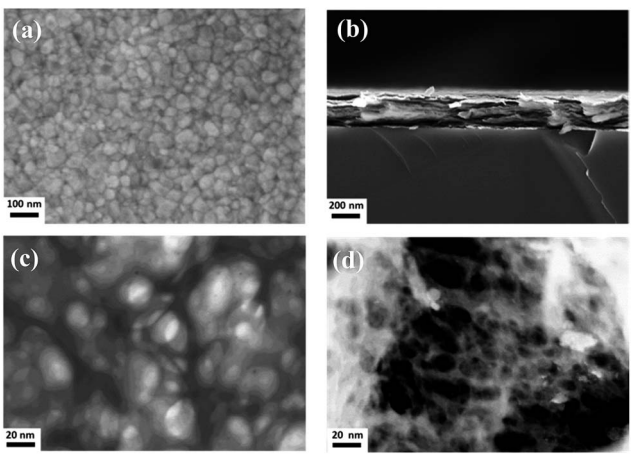

Fig. 1 Morphology of the Laponite films: (a) top-view SEM micrograph; (b) SEM cross-section showing stacks of leaflet layers perpendicular to the surface of the substrate; (c) STEM micrograph obtained on thin film areas prepared on a Ni-TEM grid. Notice the T-type bonding between the Laponite particles, *e.g.* readily visible in the center of the micrograph; (d) STEM micrograph of the nanocomposite film showing the fine structure and the mesoporous character of the film.

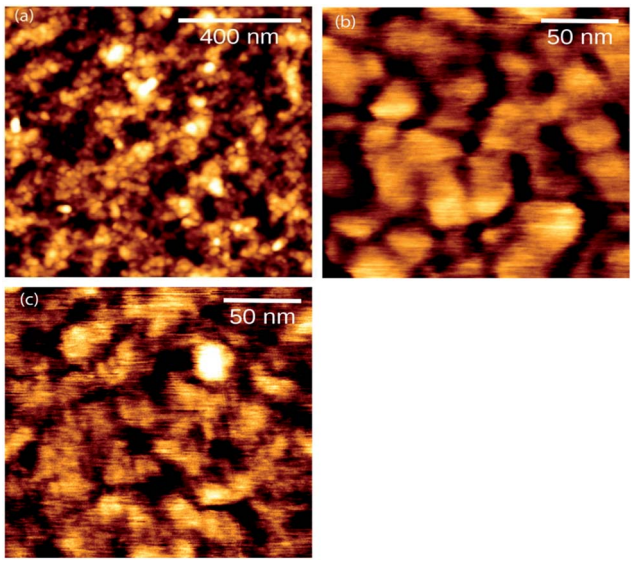

Fig. 2 AFM micrographs of Laponite and nanocomposite films: (a) morphology and ordering of the Laponite nanoparticles; (b) high magnification phase micrograph of the Laponite film; (c) phase micrograph of the nanocomposite film showing fine features (striations) that suggest different arrangement of the particles on the surface (rim up).

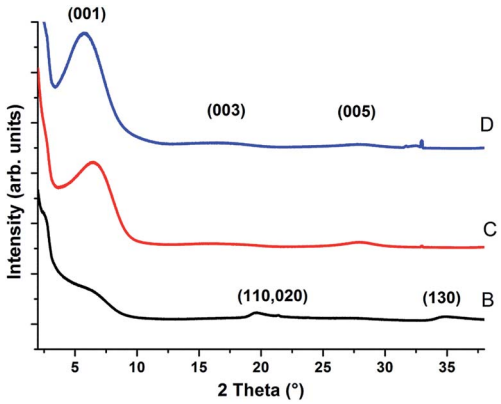

Fig. 3 XRD patterns of Laponite powder, (B), Laponite film, (C), and nanocomposite film, (D). The peaks are indexed with typical *hkl* reflections.

The mesoporous nature of the Laponite films depicted above implies a high active surface area that, coupled with low cost and easy processing, would be ideal for a double layer capacitor. This constituted the main drive to investigate the capacitive performance of the Laponite and nanocomposite film electrodes. The electrochemical properties were tested using cyclic voltammetry (CV) measurements in 1 M aqueous KCl electrolyte and a potential window from 0 of 1000 mV at various scan rates (1, 5, 10, 25, 50, and 100 mV s^{-1}). The CV behavior of the nanocomposite film electrode stabilizes after 50 cycles, and the

CV curves shown in Fig. 4 have nearly rectangular shape that indicates a good double-layer capacitive behavior under the measured scan rates, and quick dynamics of charge propagation (for the plain film see Fig. ESI-7†). The specific capacitance is calculated from the CVs using eqn (1):[14]

$$C/m = I/2VS \quad (1)$$

where C/m is the specific capacitance (F g^{-1}), I the integrated area (VA) of the CV curve in one complete cycle, V the potential window (V), S the scan rate (V s^{-1}), and m the mass (g) of the film. It should be pointed out that the mass of the film is estimated from the cross-section thickness of the film, the area of the electrode and the theoretical density of Laponite, omitting porosity. All the values calculated for the specific capacitances are therefore underestimated.

Charging–discharging experiments were conducted at constant current density, and the dependence of the specific capacitance on the scan rate is depicted in Fig. 4b that shows the well-known downward trend with increasing scan rate. At 1 mV s^{-1}, the specific capacitance obtained for the nanocomposite film is 135 F g^{-1} that is 55% higher than the 87 F g^{-1} of the plain Laponite film. These values compare well with the range of values reported for carbon-based materials, including carbon nanotubes.[15,16]

For practical applications, the galvanostatic charging–discharging behavior is more appropriate to describe the performance of the electrode. The charging–discharging curves at constant current densities, in the potential window from 0 to 0.6 V, are triangular in shape with nearly linear charging–discharging that is characteristic for double layer capacitors, and denotes good charge–discharge reversibility and nearly ideal capacitive behavior (Fig. ESI-8†). The specific capacitance can then be obtained from the slope of the charge–discharge curve according to eqn (2):

$$C/m = I\Delta t/2\Delta V \quad (2)$$

where I is the applied current (A), Δt the discharge time (s) and ΔV the potential window. Fig. 4c shows that the specific capacitance is almost constant for all the current densities investigated, with a mean value of 80 for the plain Laponite and 120 F g^{-1} for the nanocomposite film. The long term behavior was investigated at 5 A g^{-1} for 500 cycles without noticeable change in the specific capacitance, Fig. 4d.

Finally the mechanism of charge storage is briefly discussed. For thin film fabrication, Laponite particles are first dissolved in water that lead to release of Na^+ ions and negative charging of the particle faces. This charge is balanced to some degree, depending on pH, by hydroxyl ion protonation that results in a net positive charge on particle rim.[15] Particle self-assembly in the film is *via* multi-site T-type interactions (edge-to-face attractive interactions, face-to-face repulsive interaction) as unambiguously shown by the STEM micrographs depicted in Fig. 1c and d. It is obvious that this configuration results in low density films containing a high density of mesopores, and a simple geometric model of T-type bonded Laponite particles indeed shows that the void area may attain high values, depending on the angle between rim and face (see Fig. ESI-10†). The electric field driven diffusion of ions from the electrolyte into the cavities and build-up of double layers is responsible for electrochemical charge storage (non-faradaic). The higher capacitance obtained in the case of the nanocomposite film is amenable to the finer network morphology obtained with this film (*e.g.* see compare Fig. 2c and d) thus creating larger active surface. Since the CV and charge–discharge curves barely show any pseudocapacitance segments we may infer negligible contribution from the organosilane functional groups. The specific capacitance values obtained in the present work compare well with those known for double layer capacitors based on graphite with good conductivity. With respect to conductivity of Laponite we may refer to few published work on the matter which shows that Laponite is mildly conductive with ionic transport mainly governing conductivity.[17,18] This conductivity is enhanced with increasing salt and Laponite concentrations in solution.[16] Also, exchanging Na^+ with K^+ ions is known to enhance conductivity of Laponite.[17] Because we are dealing with thin film electrodes that are tested in 1 M KCl solution we may expect good conductivity of our films. Electronic conductivity of our Laponite films on which double layer behavior relies is confirmed *via* electrochemical impedance spectroscopy (Fig. ESI-9†).[19] From the Nyquist impedance plot, the charge-transfer resistance of Laponite film was calculated to be 15 Ω. This is further proof of the high capacitive performance of the Laponite films under investigation. Work is, however, in progress in order to gain more insight in the charge transport mechanisms of the Laponite films.

Based on the results presented above we can ascertain the suitability of Laponite thin films as electrode materials for

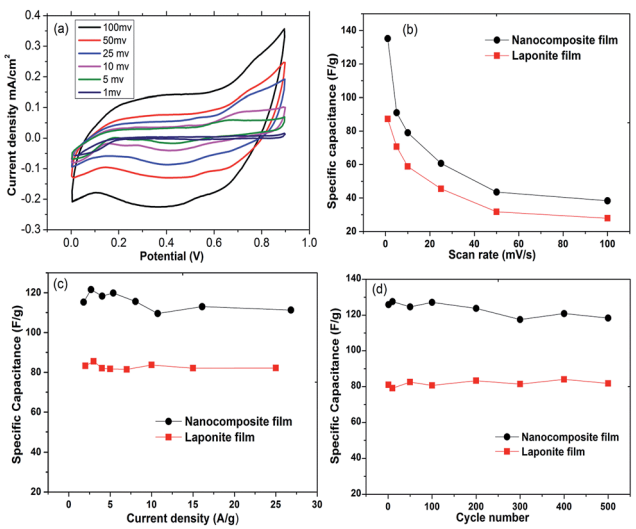

Fig. 4 (a) CVs of the nanocomposite film electrode in 1 M KCl at different scan rates; (b) plot of the specific capacitance *versus* scan rate for the Laponite and nanocomposite films. (c) The charge–discharge tests of the nanocomposite electrode in 1 M KCl at different constant current densities are shown. (d) Specific capacitance in a long-term cycling test (500 cycles) at a current density of 5 A g^{-1} for the Laponite and nanocomposite films.

energy storage applications. *Via* their structural self-assembly that yields a continuous network of mesopores Laponite films can be used as high-performance supercapacitors. Because film fabrication is from aqueous suspensions at ambient atmosphere and curing temperatures are below 100 °C the films are environmentally friendly. Further they can be deposited on electroded polymer sheets in a continuous process, thus allowing electrode coils to be fabricated, with promising potential for industrial up-scaling.

A yet another, novel application of clay materials has been shown in the present work which should pave the way for the industrial application of clay materials as low-cost, green supercapacitor electrodes. Further studies should be devoted to natural clay materials that are abundant all over the globe for sustainable resource management.

Acknowledgements

Financial support of this work is provided by the EU-program INTERREG IVA-Southern Denmark-Schleswig-K.E.R.N.-Project# 111-1.2-12 "SuperCap".

Notes and references

1 R. Stern and M. J. Jedrzejas, *Chem. Rev.*, 2008, **108**, 5061–5085.
2 M. I. Carretero and M. Pozo, *Appl. Clay Sci.*, 2010, **47**, 171–181.
3 (*a*) J. I. Dawson and R. O. C. Oreffo, *Adv. Mater.*, 2013, **25**, 4069–4086; (*b*) V. Rives, M. del Arco and C. Martín, *Appl. Clay Sci.*, 2014, **88–89**, 239–269.
4 (*a*) Z. P. Xu, J. Zhang, M. O. Adebajo, H. Zhang and Ch. Zhou, *Appl. Clay Sci.*, 2011, **53**, 139; (*b*) S. Navalon, M. Alvaro and H. Garcia, *Appl. Catal., B*, 2010, **99**, 1; (*c*) C. Belver, P. Aranda and E. Ruiz-Hitzky, *J. Mater. Chem. A*, 2013, **1**, 7477.
5 S. M. Lee and D. Tiwari, *Appl. Clay Sci.*, 2012, **59–60**, 84.
6 S. M. Liff, N. Kumar and G. H. McKinley, *Nat. Mater.*, 2007, **6**, 76.
7 V. L. Reena, C. Pavithran, V. Verma and J. D. Sudha, *J. Phys. Chem. B*, 2010, **114**, 2578.
8 (*a*) S. Letaïef, A. Martín-Luengo, P. Aranda and E. Ruiz-Hitzky, *Adv. Funct. Mater.*, 2006, **16**, 401; (*b*) H. He, Q. Tao, J. Zhu, P. Yuan, W. Shen and Sh. Yang, *Appl. Clay Sci.*, 2013, **71**, 15.
9 C. Ruiz-García, J. Pérez-Carvajal, A. Berenguer-Murcia, M. Dardera, P. Aranda, D. Cazorla-Amorós and E. Ruiz-Hitzky, *Phys. Chem. Chem. Phys.*, 2013, **15**, 18635–18641.
10 (*a*) H. van Olphen, *An Introduction to Clay Colloid Chemistry*, Wiley, New York, 1977; (*b*) M. Dijkstra, J. P. Hansen and P. A. Madden, *Phys. Rev. E: Stat. Phys., Plasmas, Fluids, Relat. Interdiscip. Top.*, 1997, **55**, 3044.
11 H. Van Olphen and J. J. Fripiat, *Data Handbook of Clay Materials and Other Non-metallic Minerals OECD and Clay Minerals Society*, Pergamon Press, New York, 1979.
12 (*a*) K. A. Carrado, *Appl. Clay Sci.*, 2000, **17**, 1; (*b*) J. D. Sudha, A. Pich, V. L. Reena, S. Sivakala and H. J. P. Adler, *J. Mater. Chem.*, 2011, **21**, 16642.
13 N. Negrete Herrera, J.-M. Letoffe, J.-P. Reymond and E. Bourgeat-Lami, *J. Mater. Chem.*, 2005, **15**, 863–871.
14 K. W. Nam and K. B. Kim, *J. Electrochem. Soc.*, 2002, **149**, 346.
15 (*a*) T. Chen and L. Dai, *Mater. Today*, 2013, **16**, 272; (*b*) D. N. Futaba, K. Hata, T. Yamada, T. Hiraoka, Y. Hayamizu, Y. Kakudate, O. Tanaike, H. Hatori, M. Yumura and S. Iijima, *Nat. Mater.*, 2006, **5**, 987.
16 M. Es-Souni, D. Schopf, C.-L. Solterbeck and M. Dietze, *RSC Adv.*, 2014, **4**, 17748.
17 A. Shahin and Y. Joshi, *Langmuir*, 2012, **28**, 15674.
18 R. C. Greaves, S. P. Bond and W. R. McWhinnie, *Polyhedron*, 1995, **14**, 3635.
19 (*a*) K. Liang, X. Tang and W. Hu, *J. Mater. Chem.*, 2012, **22**, 11062–11067; (*b*) G. Han, Y. Liu, E. Kan, J. Tang, L. Zhang, H. Wang and W. Tang, *RSC Adv.*, 2014, **4**, 9898–9904.